Interfacial Charge-Transfer Absorption: Semiclassical Treatment

Carol Creutz,*,† Bruce S. Brunschwig,*,‡ and Norman Sutin*,†

Chemistry Department, Brookhaven National Laboratory, Upton, New York 11973-5000, and Beckman Institute, California Institute of Technology, Mail Code 139-74, 1200 East California Boulevard, Pasadena, California 91125

Received: January 14, 2005; In Final Form: March 29, 2005

Optically induced charge transfer between adsorbed molecules and a metal electrode was predicted by Hush to lead to new electronic absorption features but has not been experimentally observed. However, Gerischer characterized photocurrents arising from such absorption between adsorbed metal atoms and semiconductor conduction bands. Interfacial charge-transfer absorption (IFCTA) provides information concerning the barriers to charge transfer between molecules and the metal/semiconductor and the magnitude of the electronic coupling and could thus provide a powerful tool for understanding interfacial charge-transfer kinetics. Here we provide a framework for modeling and predicting IFCTA spectra. The key feature of optical charge transfer to or from a band of electronic levels (taken to have a constant density of states and electronic coupling element) is that the absorption probability reaches half intensity at $\lambda + \Delta G^{\theta}$, where λ and ΔG^{θ} are the reorganization energy and free-energy gap for the optical charge transfer, attains >90% intensity at $\lambda + \Delta G^{\theta} + 0.9\sqrt{4\lambda k_B T}$, and remains essentially constant until the top (bottom) level of the band is attained. However, when the electronic coupling and transition moment are assumed to be independent of photon energy (Mulliken−Hush model), a peaked, highly asymmetric absorption profile is predicted. We conclude that, in general, the electronic coupling between molecular adsorbates and the metal levels is so small that absorption is not detectable, whereas for semiconductors there may be intense features involving coupling to surface states.

I. Introduction

There is presently much effort directed toward characterizing and modeling the interfacial charge transfer from molecular species to metals and semiconductors.[1] For the case of bulk metal electrodes, electrochemical methods have been used to study electron transfer to/from a molecular acceptor/donor located at the end of a thiolate attached to the electrode as part of a self-assembled monolayer.[2−4] The distance dependences of both the reorganization barrier λ and the electronic coupling H_{12} for the electron transfer have been extracted from the rate measurements. Thermal electron transfer to/from semiconductor electrodes depends on the carrier density.[5] For the case of bulk and nanocrystalline *n*-type semiconductor TiO_2, the kinetics of both electron photoinjection and back reaction in dye-TiO_2,[6−9] ZrO_2,[10] and ZnO[11] assemblies have been investigated. However, because both processes are complex the level of modeling is not now as advanced as for the metals. The understanding of molecular electron-transfer reactions has been enhanced through spectroscopic studies of molecular donor−acceptor pairs. This area has been most broadly explored for mixed-valence systems[12−15] for which, following the framework given by Hush[14,15] and Mulliken,[12,13] the band maxima and integrated intensities of binuclear transition-metal complexes,[16−19] ion pairs,[20,21] and organic redox couples[22−26] have been compared with activation barriers and rates for thermal electron-transfer reactions.[27] Such a spectroscopic approach would seem to offer a powerful probe of solute or adsorbate interactions with metal and semiconductor electrodes, especially for nanoparticle systems where the relative surface areas are very large. Indeed, optical charge transfer between metal adatoms and CdS and ZnO semiconductor electrodes[28] and between adsorbed ferrocyanide ion[6,29,30] or catechol[31−35] and TiO_2 nanoparticles has been reported.

Interfacial charge-transfer absorption (IFCTA) from solute metal ions to metallic electrodes was predicted by Hush in 1968,[15,36,37] although to our knowledge no such absorption bands have been reported. Hush did not, however, include the band structure of the metal, which, as will be seen, has a profound effect on the predicted absorption profile. In addition, the Hush treatment was limited to metals. Because both semiconductors and metals possess closely spaced occupied electronic levels and closely spaced unoccupied levels, a common framework (with due attention to the differences in the properties of the two kinds of material) is appropriate for their interfacial charge-transfer processes. As developed by Hush, the interfacial charge-transfer bands were expected to be extremely weak and to lie at long wavelengths (in some cases in the near-infrared or infrared regions), thus making their observation experimentally very challenging. The recent emergence of metal and semiconductor nanoparticles provides a new opportunity to study molecular−interfacial charge-transfer absorption spectra; the nanoparticles have many sites for the adsorption of molecular donors/acceptors so that the probability of charge-transfer absorption is increased relative to that of comparable adsorption on a bulk material. Furthermore, it is experimentally more straightforward to examine nanoparticle solutions than bulk-solute/adsorbate interfaces.

In this article, we consider the features that would be expected for such interfacial charge-transfer absorption features for the bulk material and for nanoparticles. Our approach here is

* Corresponding author. E-mail: ccreutz@bnl.gov; bsb@caltech.edu; sutin@bnl.gov.
† Brookhaven National Laboratory.
‡ Beckman Institute.

10.1021/jp050259+ CCC: $30.25
Published on Web 04/28/2005

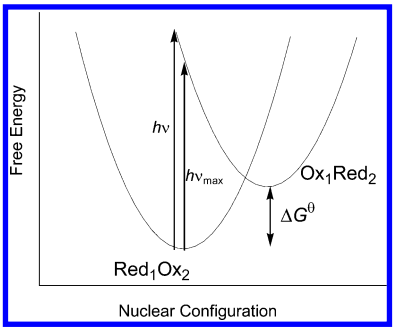

Figure 1. Reactant Red_1Ox_2 and product Ox_1Red_2 surfaces for intramolecular electron transfer: free energy as a function of the nuclear coordinate.

semiclassical: We use expressions for thermal and optical electron-transfer processes that are based on Fermi's golden rule, but with the density of states (Franck−Condon factor) of the redox couple treated within the Marcus framework. In the following sections, we first compare optical and thermal electron transfer in molecular systems and then replace one molecular redox partner with a metal or a semiconductor. Finally, we discuss the absorption profiles to be expected for different electronic coupling mechanisms.

II. Model for Interfacial Charge-Transfer Absorption (IFCTA)

A. Comparison of Optical and Thermal Processes for Intramolecular Electron Transfer. To begin, we consider the parallel between thermal and optical intramolecular electron transfer in a binuclear system containing sites 1 and 2 and the electron-transfer process

$$Red_1Ox_2 \rightarrow Ox_1Red_2 \tag{1}$$

depicted in Figure 1.

The rate constant for the Red_1-to-Ox_2 electron transfer derived utilizing a transition-state theory approach is given by[38,39]

$$k_{12} = \left(\frac{4\pi^2}{h}\right)(H_{12})^2\left[\frac{1}{(4\pi\lambda_{12}k_BT)^{1/2}}\right]\exp\left[-\frac{[\lambda_{12} + \Delta G_{12}{}^{\theta}]^2}{4\lambda_{12}k_BT}\right] \tag{2}$$

where H_{12} is the electronic coupling element, λ_{12} is the reorganization energy, and ΔG_{12}^{θ} is the free-energy difference between the equilibrium configurations of the reactants and products.

$$\lambda_{12} = \lambda_1 + \lambda_2 \tag{3a}$$

$$\lambda_1 = \lambda_{ox,1} + \lambda_{red,1} \tag{3b}$$

$$\lambda_2 = \lambda_{ox,2} + \lambda_{red,2} \tag{3c}$$

$$\Delta G_{12}^{\theta} = -e(E_2^0 - E_1^0) \tag{4}$$

(Note that eq 3a breaks down when the solvent reorganization contribution is significant and reactants 1 and 2 differ significantly in size.) It is apparent from eq 2 that a plot of k_{12} versus ΔG_{12}^{θ} for a series of homologous reactions in which λ_{12} and H_{12} are constant will be Gaussian-shaped with a maximum at $-\Delta G_{12}^{\theta} = \lambda_{12}$ and a full width at half-height given by[40]

$$\Delta\nu_{1/2} = 2[4\ln(2)\lambda_{12}k_BT]^{1/2} \tag{5}$$

Equation 2 is applicable provided that the interaction of the reactants and products is weak and that the energy of the system is adequately described by zero-order parabolic surfaces. It is also the high-temperature limit of fully quantum-mechanical treatments.[41]

Turning to optical charge transfer, as long as the ground-state surface is parabolic and the population of systems on the ground-state energy surface is Boltzmann (an assumption also made in the transition-state treatment) the distribution of molecules per unit spectral energy interval as a function of the vertical energy difference between the ground and excited state will be given by a Gaussian

$$\frac{n_A}{[Red_1Ox_2]} = \frac{1}{\sqrt{4\pi\lambda_{12}k_BT}}\exp\left[-\frac{(\lambda_{12} + \Delta G_{12}^{\theta} - h\nu)^2}{4\lambda_{12}k_BT}\right] \tag{6a}$$

where $[Red_1Ox_2]$ is the total concentration of the Red_1Ox_2 system and n_A is the concentration of Red_1Ox_2 systems that have a given vertical energy difference, $h\nu$, between the ground and excited states. Consequently, provided that the intrinsic absorptivity of the system is independent of the nuclear configuration of the ground state then the absorption of the system will be proportional to n_A. This leads to the following expression for the molar absorptivity ϵ_ν[42]

$$\frac{\epsilon_\nu}{\nu} = \left(\frac{\epsilon_\nu}{\nu}\right)_{max}\exp\left[-\frac{(\lambda_{12} + \Delta G_{12}^{\theta} - h\nu)^2}{4\lambda_{12}k_BT}\right] \tag{6b}$$

where $(\epsilon_\nu/\nu)_{max}$ is a function of λ_{12} and the transition dipole moment and is discussed later. For a symmetric molecular system, $\Delta G_{12}^{\theta} = \Delta G_{21}^{\theta} = 0$ and the maximum in the intervalence charge-transfer spectrum occurs at λ_{12}. Were it possible to vary the free-energy change ΔG_{12}^{θ} continuously, the resulting plot of rate constant versus free-energy change (eq 2) would be the same shape and have the same width as the corresponding charge-transfer absorption spectrum for any particular value of ΔG_{12}^{θ}. Each point on the rate-constant plot would correspond to a different redox pair $(Red_1Ox_2)_i$ with $-\Delta G_{12,i}^{\theta} = \Delta G_{21,i}^{\theta}$, and each reaction product $(Ox_1Red_2)_i$ will exhibit intervalence charge-transfer absorption with the same Gaussian and half-width centered at $h\nu_{max} = \lambda_{12} + \Delta G_{21,i}^{\theta}$. This is illustrated in Figure 2 for systems at $-\Delta G_{12,i}^{\theta} = \lambda_{12}$, $2\lambda_{12}$, and $3\lambda_{12}$ along the rate-constant curve.

Single Couple Surfaces. Instead of considering the thermal electron transfer in terms of two energy surfaces, one for the reactants and the other for the products, as in Figure 1, the redox couples can be considered separately because within a weak coupling model their interaction can be neglected. For the electron transfer discussed above, the reducing and oxidizing couples are

$$Red_1 \rightarrow Ox_1 + e^-(vac) \tag{7a}$$

$$Ox_2 + e^-(vac) \rightarrow Red_2 \tag{7b}$$

and the energy surfaces for the various species are shown in Figure 3.

Moreover, rather than considering the reaction as proceeding via "activation" of the reactants and formation of an activated complex or transition state, the progress of the reaction can be considered in terms of the vertical differences between the energies of the oxidized and reduced forms of the two couples.[43] Analogous to eq 6, the distributions of species Red_1 or Ox_2 as a function of the vertical energy differences ΔG_{v1} for

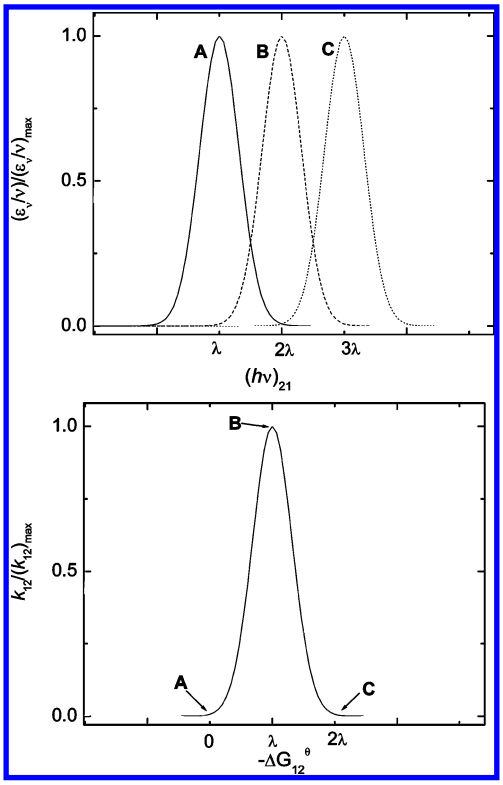

Figure 2. (Bottom) Plot of the normalized rate constant for thermal $Red_1Ox_2 \rightarrow Ox_1Red_2$ electron transfer vs driving force $-\Delta G_{12}^{\theta}$. (Top) $(Ox_1Red_2)_i \rightarrow (Red_1Ox_2)_i$ charge-transfer spectra with maxima at $\lambda + \Delta G_{21,i}^{\theta}$ for points A, B, and C of the lower plot.

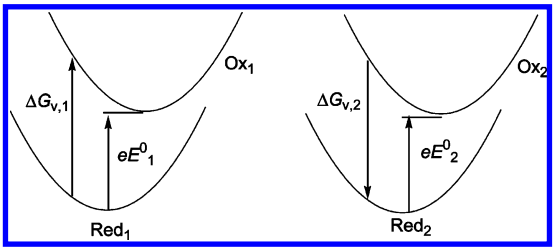

Figure 3. Energy surfaces for the individual couples in eq 1; free energy as a function of the nuclear configuration of 1 (left) and 2 (right).

$Red_1 - Ox_1$ and ΔG_{v2} for $Ox_2 - Red_2$ have a Gaussian form

$$D_{1,\mathrm{red}} = \left[\frac{1}{(4\pi\lambda_1 k_B T)^{1/2}}\right] \exp\left[-\frac{[\lambda_1 + eE_1^0 - \Delta G_{v,1}]^2}{4\lambda_1 k_B T}\right] \quad (8a)$$

$$D_{2,\mathrm{ox}} = \left[\frac{1}{(4\pi\lambda_2 k_B T)^{1/2}}\right] \exp\left[-\frac{[\lambda_2 + eE_2^0 - \Delta G_{v,2}]^2}{4\lambda_2 k_B T}\right] \quad (8b)$$

where $D_{1,\mathrm{red}}$ and $D_{2,\mathrm{ox}}$ are the distribution functions or density of states for the reductant (occupied state) and oxidant (unoccupied state), respectively, eE_j^0 is the free-energy difference between the minima of the oxidized and reduced forms of couple j, $\Delta G_{v,1}$ is the energy *required* to remove an electron from Red_1 at constant nuclear configuration, and $\Delta G_{v,2}$ is the energy *released* when Ox_2 accepts the electron at constant nuclear configuration (Figure 3). Conservation of energy requires that when electron transfer takes place between the species the vertical energy differences must be equal (i.e., $\Delta G_{v,1} = \Delta G_{v,2}$). The probability of the electron transfer taking place at a given ΔG_v is given classically by the product of the number of each species that have the particular energy difference

$$P(\Delta G_v) = D_1(\Delta G_v)\, D_2(\Delta G_v) \quad (9a)$$

The total probability of electron transfer is then just the sum of the individual contributions

$$P = \int_{-\infty}^{\infty} P(\Delta G_v)\, \mathrm{d}(\Delta G_v)$$
$$= \left(\frac{1}{(4\pi\lambda_1 k_B T)}\right)\left(\frac{1}{(4\pi\lambda_2 k_B T)}\right] \int \exp$$
$$\left[-\frac{(\lambda_1 + eE_1^0 - \Delta G_{v,2})^2}{4\lambda_1 k_B T} - \frac{(\lambda_2 - eE_2^0 - \Delta G_v)^2}{4\lambda_2 k_B T}\right] \mathrm{d}(\Delta G_v) \quad (9b)$$

The integral of the product of two Gaussians is a Gaussian with the result that the probability of electron transfer is given by

$$P = \int_{-\infty}^{+\infty} D_1 D_2\, \mathrm{d}(\Delta G_v) =$$
$$\left[\frac{1}{(4\pi\lambda_{12} k_B T)^{1/2}}\right] \exp\left[-\frac{(\lambda_{12} + \Delta G_{12}^{\theta})^2}{4\lambda_{12} k_B T}\right] \quad (9c)$$

This is the same nuclear reorganization (Franck−Condon) factor as in eq 2.[44] Thus, the parallel between thermal and optical electron transfer is readily evident when the thermal reaction, like the optical transfer, is considered in terms of vertical energy differences.[45−47] In this regard, the activated electron transfer can be seen as a zero-energy optical transition.

B. Thermal and Optical Electron Transfer to/from Metals. A similar relationship between the expressions for optical and thermal electron transfer is obtained for electron transfer between a redox couple and a metal. However, in contrast to the previous case, a redox couple and a *band* of filled and empty levels is involved. First consider *thermal* charge transfer to and from electronic levels B of a metal electrode and those of a molecular electron donor (reductant Red) or electron acceptor (oxidant Ox).

$$B(e^-) + Ox \rightleftharpoons B() + Red \quad (10a)$$

$$B(e^-) - Ox \underset{k_{RB}}{\overset{k_{BO}}{\rightleftharpoons}} B() - Red \quad (10b)$$

The driving force for electron transfer from level ϵ_i of a metal to a molecular acceptor with reduction potential E^0 is

$$\Delta G_i^0(\mathrm{BO}) = e(E_i - E^0) \quad (11)$$

$$E_i = E_F - \frac{\epsilon_i}{e} \quad (12a)$$

$$\epsilon_i = \epsilon_i' - \epsilon_F' \quad (12b)$$

where E_i is the quasi or effective electrode potential of the metal (for electron transfer to or from level i), E_F is the "normal" electrode potential of the metal (for electron transfer to or from the Fermi level), and ϵ_i' and ϵ_F' are the energies of level i and of the Fermi level relative to a common reference, usually the vacuum. The Fermi energy is the energy of the level for which the probability that the level will be occupied is $^1/_2$. For the reverse process—transfer from a molecular donor with reduction potential E^0 to an unoccupied level ϵ_i of a metal—the driving force is

$$\Delta G_i^0(\mathrm{RB}) = -e(E_i - E^0) \quad (13)$$

As in the intramolecular case, electron transfer can occur only when the energy of an occupied donor state matches that of an unoccupied receiver state. Thus, the forward and reverse rate constants are obtained from the overlaps of the distribution functions for the molecular reagent (D_{ox}, D_{red}) and the electrode ($D_{B(e)}$ and $D_{B()}$)[43,48,49] for the forward (k_f) and reverse (k_r) processes, respectively:

$$k_{BO} = \frac{4\pi^2}{h}(H_{ab})^2 \int_{-\infty}^{+\infty} D_{B(e)}\, D_{ox}(\epsilon_i)\, d\epsilon_i = \frac{4\pi^2}{h}(H_{ab})^2 \int_{-\infty}^{+\infty} \rho(\epsilon_i)\, f(\epsilon_i)\, D_{ox}(\epsilon_i)\, d\epsilon_i \quad (14a)$$

$$k_{RB} = \frac{4\pi^2}{h}(H_{ab})^2 \int_{-\infty}^{+\infty} D_{B(\,)}\, D_{red}(\epsilon_i)\, d\epsilon_i = \frac{4\pi^2}{h}(H_{ab})^2 \int_{-\infty}^{+\infty} \rho(\epsilon_i)[1 - f(\epsilon_i)] D_{red}(\epsilon_i)\, d\epsilon_i \quad (14b)$$

where $\rho(\epsilon_i)$ is the density of states per energy per atom in the electrode, $f(\epsilon_i)$ is the electron occupancy factor given by the Fermi−Dirac distribution

$$f(\epsilon_i)_{oc} = \frac{1}{1 + \exp\left(\frac{\epsilon_i}{k_B T}\right)} \quad (15)$$

and, as before (eq 12b), ϵ_i is the energy of level i relative to the energy of the Fermi level. Within the Marcus treatment, the distribution functions for the oxidized and reduced forms of the couple are the Gaussians given by eq 8 where, for energy conservation, $\Delta G_v = \pm e(E_i)$ with E_i given by eq 12:

$$D_{ox}(\epsilon_i) = \left[\frac{1}{(4\pi\lambda k_B T)^{1/2}}\right] \exp\left[-\frac{[\lambda + e(E_i - E^0)]^2}{4\lambda k_B T}\right] \quad (16a)$$

$$D_{red}(\epsilon_i) = \left[\frac{1}{(4\pi\lambda k_B T)^{1/2}}\right] \exp\left[-\frac{[\lambda - e(E_i - E^0)]^2}{4\lambda k_B T}\right] \quad (16b)$$

The maxima of the two distributions are at $eE_i = eE^0 - \lambda$ and $eE_i = eE^0 + \lambda$, respectively, and are separated by 2λ. The distribution functions for the redox couple and the metal are depicted in Figure 4.

The rate constants for the forward and reverse electron transfers obtained by integrating over all of the energy levels of the electrode are then[3,50,51]

$$k_{BO} = \frac{4\pi^2}{h}\frac{(H_{ab})^2}{\sqrt{4\pi\lambda k_B T}}\rho_M \int_{-\infty}^{+\infty} f(\epsilon_i) \exp\left[-\frac{(\lambda - \epsilon_i + e(E_F - E^0))^2}{4\lambda k_B T}\right] d\epsilon_i \quad (17)$$

$$k_{RB} = \frac{4\pi^2}{h}\frac{(H_{ab})^2}{\sqrt{4\pi\lambda k_B T}}\rho_M \int_{-\infty}^{+\infty} [1 - f(\epsilon_i)] \exp\left[-\frac{(\lambda + \epsilon_i - e(E_F - E^0))^2}{4\lambda k_B T}\right] d\epsilon_i \quad (18)$$

where ϵ_i is given by eq 12b and H_{ab} and the density of states ρ_M in the electrode are assumed to be independent of energy. The integral over all ϵ_i shown in eqs 17 and 18 is the overlap of a single Gaussian with either the occupied or unoccupied

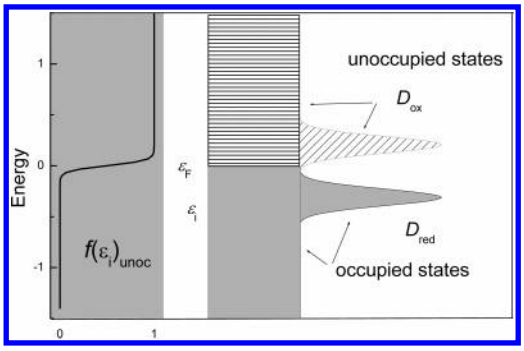

Figure 4. Distribution functions for molecular reactants (D_{ox}, D_{red}) and a metal electrode with Fermi level ϵ_F. At the left, the electron unoccupancy factor, $f(\epsilon_i)_{unoc} = 1 - f(\epsilon_i)$, is depicted where $f(\epsilon_i)$ is the occupancy factor of the level. Adapted from ref 48.

levels of the bulk metal. The Gaussian shifts to higher (lower) energy as the driving force ($\pm e(E_f - E^0)$) is changed. The rate profile, a plot of k_{BO} versus $\Delta G^\theta_{BO} = e(E_F - E^0)$ or k_{RB} versus $\Delta G^\theta_{RB} = -e(E_F - E^0)$, given by eqs 17 and 18, respectively, is not Gaussian but rather exhibits a plateau for $|\Delta G^\theta| \geq 2\lambda$ (a consequence of the fact that the overlap is between a Gaussian and a Fermi function rather than between two Gaussians as is the case of the intramolecular electron transfer[49]). Thus, as is well known, the Marcus inverted regime found for highly exergonic intramolecular electron-transfer reactions is not observed for molecule−metal−electrode reactions.

Analogous to the thermal reactions, two light-induced electron transfers are expected: an electron may be promoted from a reductant to any of the unoccupied metal levels. In addition, an electron may be promoted from an occupied metal level to an oxidant (Figure 5).

The above processes are entirely analogous to charge-transfer absorption within and between molecules except that the metal levels form part of a band of closely spaced levels rather than energetically well separated molecular orbitals. To emphasize that a band of levels is involved, we denote optical charge transfer from an electron donor as reductant-to-band (RBCT) and to an electron acceptor as band-to-oxidant charge transfer (BOCT).

For the case of optically induced electron transfer from a molecular donor with reduction potential E^0 to an unoccupied level ϵ_i of a metal, ΔG^0_i is

$$\Delta G^0_i(\mathrm{RBCT}) = -e(E_i - E^0) = \epsilon_i - e(E_F - E^0) \quad (19)$$

whereas for the analogous case of optically induced electron transfer from an occupied level ϵ_i of a metal to a molecular acceptor with reduction potential E^0, ΔG^θ_i is given by

$$\Delta G^0_i(\mathrm{BOCT}) = e(E_i - E^0) = -\epsilon_i + e(E_F - E^0) \quad (20)$$

where E_i is the effective electrode potential of the metal defined by eq 12 and E_F is the normal electrode potential of the metal.

The above treatment predicts that the absorption band deriving from electron transfer to or from a single energy level ϵ_i of the metal will be Gaussian with ϵ_ν/ν given by

$$\left(\frac{\epsilon_\nu}{\nu}\right)_i^{\mathrm{RBCT}} = \left(\frac{\epsilon_\nu}{\nu}\right)_{\max}^{\mathrm{RBCT}} \sqrt{4\pi\lambda k_B T}[1 - f(\epsilon_i)] D_{red}(\epsilon_i) \quad (21a)$$

$$\left(\frac{\epsilon_\nu}{\nu}\right)_i^{\mathrm{BOCT}} = \left(\frac{\epsilon_\nu}{\nu}\right)_{\max}^{\mathrm{BOCT}} \sqrt{4\pi\lambda k_B T} f(\epsilon_i)\, D_{ox}(\epsilon_i) \quad (21b)$$

$$\sqrt{4\pi\lambda k_B T}D_{red/ox}(\epsilon_i) = \exp\left[\frac{-(\lambda + \Delta G_i^0 - h\nu)^2}{4\lambda k_B T}\right] = \exp\left[\frac{-((h\nu)_{max} - h\nu)^2}{4\lambda k_B T}\right] \quad (22)$$

where ϵ_ν is the molar absorptivity at transition energy $h\nu$, the maximum of the Gaussian is

$$(h\nu)_{max} = \lambda + \Delta G_i^0 \quad (23)$$

with ΔG_i^0 given by eq 19 or 20, and its half-width is $\Delta\nu_{1/2} = 2[4\ln(2)\lambda k_B T]^{1/2}$ (cf. eq 5). We note that the prefactor $(\epsilon_\nu/\nu)_{max}$ is assumed to be independent of the particular level used (section E).

The above expressions pertain to a single filled or empty level ϵ_i of the metal. Figure 6 illustrates contributions from several component levels for a metal, with all transition maxima assumed to have identical intrinsic intensities. Normally, RBCT absorptions have contributions for charge transfer to all unoccupied levels of the metal (primarily above the Fermi level), whereas BOCT bands have contributions from all of the metal occupied levels (primarily below the Fermi level). The total observed absorbance is then the sum of the contributions from all of the transitions to (from) the individual levels. For RBCT absorption, the lowest-energy absorption arises from charge transfer of vibrationally hot R molecules to the unoccupied levels of the metal below the Fermi level. Because the populations of both the vibrationally hot molecules and these lowest-energy unoccupied bands are very low, the absorbance at low energy is small. However, as the photon energy increases the absorption becomes dominated by transitions from molecules close to their equilibrium nuclear configuration into the numerous unoccupied bands above the Fermi level. Further increases in photon energy increase the metal level into which charge is transferred. There are contributions to the absorption profile from charge transfer into levels up to the top of the conduction band. Although it would be expected that above this energy the absorbance should decrease because of the width of the band (3 eV or more), this cutoff might not be readily observed. The BOCT charge-transfer process gives rise to a similar absorption profile.

The total absorption profile is given by the summation of the individual transitions. If the metal levels ϵ_i are taken as a continuum of states, with a density of states per energy of ρ_M assumed to be independent of energy, then the following expressions are obtained:

$$\left(\frac{\epsilon_\nu}{\nu}\right)^{RBCT} = \left(\frac{\epsilon_\nu}{\nu}\right)^{RBCT}_{max} \rho_M \int_{-\infty}^{+\infty} \frac{\exp[-(\lambda - h\nu + \epsilon_i - e(E_F - E^0))^2/4\lambda k_B T]}{[1 + \exp(-\epsilon_i/k_B T)]} d\epsilon_i \quad (24a)$$

$$\left(\frac{\epsilon_\nu}{\nu}\right)^{BOCT} = \left(\frac{\epsilon_\nu}{\nu}\right)^{BOCT}_{max} \rho_M \int_{-\infty}^{+\infty} \frac{\exp[-(\lambda - h\nu - \epsilon_i + e(E_F - E^0))^2/4\lambda k_B T]}{[1 + \exp(\epsilon_i/k_B T)]} d\epsilon_i \quad (24b)$$

The resulting absorption profile is shown in Figure 7.

The key feature of optical charge transfer to or from a band of electronic levels (taken to have a constant density of states and electronic coupling) is that the absorption profile is given by the profile in Figure 7 in which the absorption probability reaches half intensity at $h\nu = \lambda + \Delta G^\theta$, attains >90% intensity at $\lambda + \Delta G^\theta + 0.9\sqrt{4\lambda k_B T}$, and remains essentially constant until the top (bottom) metal level is attained. Thus, just as the intervalence charge-transfer spectrum and the intramolecular electron-transfer rate constant as a function of ΔG^θ may both be cast as the integral over the product of $D_{red,1}$ and $D_{ox,2}$,[47] which is a Gaussian, the integral of eq 24, the product of the distribution functions for the metal/electrode and the molecule, gives both the rate profile for electron transfer to the metal and the BCT spectrum. (Note that the rate profile corresponding to Figure 7 has been observed in a number of experiments.[3,4,52−56])

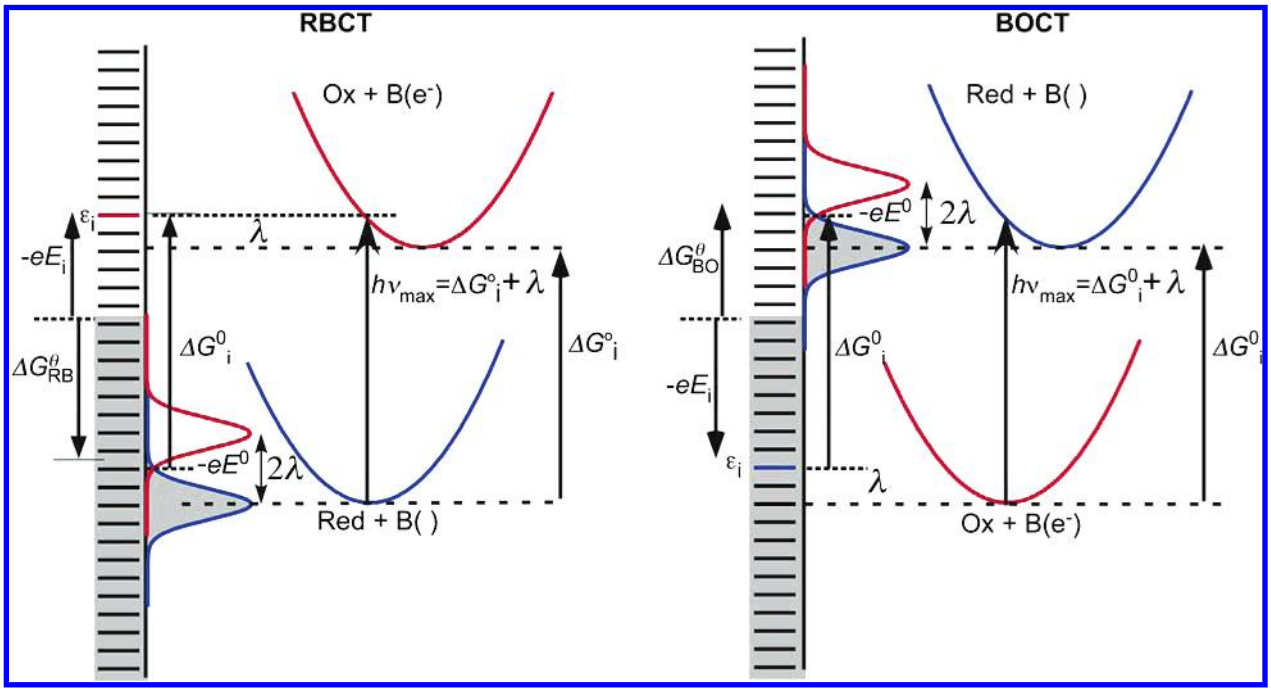

Figure 5. (a) Light absorption may induce electron transfer from the molecular reductant to an empty energy level of the metal, that is, from the initial Red + B() state to the final Ox + B(e^-) state. (b) Light-induced electron transfer from a filled level of the metal or semiconductor to a molecular oxidant, that is, from the B(e^-) + Ox state to the B() + Red state.

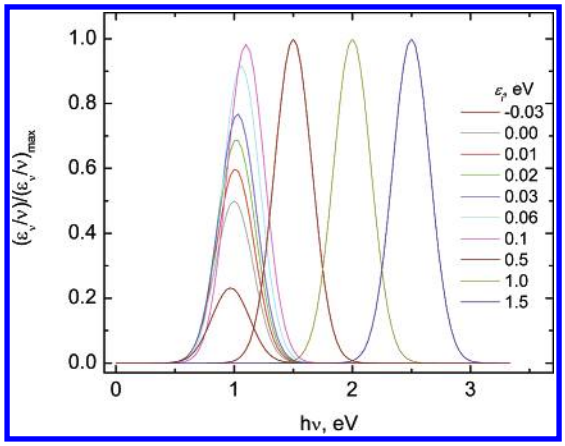

Figure 6. Selected Gaussian components corresponding to optical electron transfer from R to individual unfilled metal levels at ϵ_i; RBCT spectrum calculated for $\lambda = 0.5$ eV, $\Delta G^\theta - e(E_F - E^0) = 0.5$ eV, $T = 298$ K.

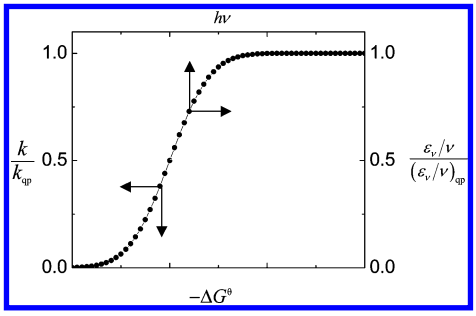

Figure 7. Comparison of normalized thermal (k/k_{qp} vs $-\Delta G^\theta$, line; bottom and left axes) and optical ($\epsilon_\nu/\nu/(\epsilon_\nu/\nu)_{qp}$ vs $h\nu$, ●; top and right axes) electron transfer between a molecule and a metal. Ratios k/k_{qp} and $\epsilon_\nu/\nu/(\epsilon_\nu/\nu)_{qp}$ attain half of their quasi-plateau (qp) values at $-\Delta G^\theta = \lambda$ and $h\nu = \Delta G^\theta + \lambda$, respectively.

For a stable molecular redox couple, both RBCT and BOCT should be observable. At a metal electrode potentiostated at the E^0 for the couple, the concentrations of oxidized and reduced forms will be equal, and the RBCT and BOCT spectra will be superposed; however, in general their maxima will be separated by an energy of $|2\Delta G^\theta|$. As noted by Hush,[15] changing the potential will alter the concentration ratio according to the Nernst equation and shift the relative absorption intensities of the two charge-transfer transitions. The relative intrinsic intensities of the transitions will in general depend on the degeneracy of the donor HOMO and the acceptor LUMO and on the magnitude of the electronic coupling to be considered below.

C. Optical Electron Transfer to/from Semiconductors. As noted earlier, for semiconductors the bands of filled levels (valence band) and unoccupied levels (conduction band) are separated by an energy gap ΔE_g (Figure 8).

In contrast to metals, where the excess charge resides on the surface, the excess charge on semiconductors extends into their interior, giving rise to a space-charge region within the semiconductor. As a consequence, there are electrical double layers on either side of a semiconductor/solution interface. The higher charge density and capacity of the double layer on the solution side results in almost all of the potential difference between the semiconductor and the solution occurring across the semiconductor's space-charge region that is being reflected in the bending of the semiconductor bands.[43,57,58] The bands are bent upward at the surface of an *n*-type semiconductor that has acquired a positive charge (and an electron-depletion layer) as a result of electron transfer to an oxidant or the application of a positive potential. However, transfer of excess electrons to

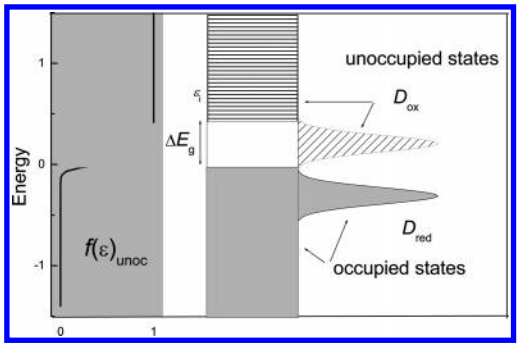

Figure 8. Distribution functions for molecular reactants (D_{ox}, D_{red}) and a semiconductor electrode with gap ΔE_g. At the left, the electron unoccupancy factor, $f(\epsilon_i)_{unoc} = 1 - f(\epsilon_i)$, is depicted. Adapted from ref 48.

the semiconductor or application of a negative potential results in the downward bending of the bands at the surface and the formation of an electron-accumulation layer. In either case, the applied potential simply increases or decreases the degree of band bending. In the absence of a high concentration of surface states, the bands may remain fixed or "pinned" at the semiconductor surface. Under these conditions, the potential difference across the semiconductor/solution interface will remain constant, independent of the applied potential.

Electron-depleted *n*-type semiconductors are widely used in photoinjection studies because the field gradient at the surface of the semiconductor efficiently removes the injected electron from the interface, thereby slowing down charge recombination. In terms of the above model, ΔG_i^0 for optically induced electron transfer from an electron donor to a level in the conduction band of an *n*-type semiconductor (which is the class of systems most frequently studied) is given by

$$\Delta G_i^0(\text{RBCT}) = -e(E_i^{CB} - E^0) \tag{25a}$$

$$E_i^{CB} = -\left(E_{bot}^{CB} - \frac{\epsilon_i^{CB}}{e}\right) \tag{25b}$$

where E^0 is the standard potential of the redox couple on the vacuum scale, E_i^{CB} and E_{bot}^{CB} are the effective potentials of the semiconductor for electron transfer to or from the *i*th level of the conduction band and the bottom level of the conduction band, respectively, and ϵ_i^{CB} is the difference between the energy of the *i*th level and the bottom level of the conduction band. Similarly, ΔG_i^0 for optically induced electron transfer from the edge (top) of the valence band to an electron acceptor is given by

$$\Delta G_i^0(\text{BOCT}) = e(E_i^{VB} - E^0) \tag{26a}$$

$$E_i^{VB} = \left(E_{top}^{VB} - \frac{\epsilon_i^{VB}}{e}\right) \tag{26b}$$

where E_i^{VB} and E_{top}^{VB} are the effective potentials of the semiconductor for electron transfer to or from the *i*th valence band and the highest (top) level of the valence band, respectively, and ϵ_i^{VB} is the difference in energy between the *i*th level of the valence band and the top of the valence band.

For many semiconductors, the Fermi−Dirac population function can be replaced by a step function[59,60] because the transition between empty and filled states occurs in the band gap region where there are very few states. Then eq 21 reduces to the following expressions for RBCT and BOCT, respectively:

$$\left(\frac{\epsilon_\nu}{\nu}\right)_{i,\mathrm{unoc}}^{\mathrm{RBCT}} = \left(\frac{\epsilon_\nu}{\nu}\right)_{\max}^{\mathrm{RBCT}} \sqrt{4\pi\lambda k_\mathrm{B}T}(D_{\mathrm{red}}(\epsilon_i))_{i,\mathrm{unoc}} \qquad \epsilon_i > \epsilon_{\mathrm{bot}}^{\mathrm{CB}} \tag{27a}$$

$$\left(\frac{\epsilon_\nu}{\nu}\right)_{i,\mathrm{oc}}^{\mathrm{BOCT}} = \left(\frac{\epsilon_\nu}{\nu}\right)_{\max}^{\mathrm{BOCT}} \sqrt{4\pi\lambda k_\mathrm{B}T}(D_{\mathrm{ox}}(\epsilon_i))_{i,\mathrm{oc}} \qquad \epsilon_i < \epsilon_{\mathrm{top}}^{\mathrm{VB}} \tag{27b}$$

provided that $|\epsilon_i - \epsilon_\mathrm{F}|$ is greater than 0.1 eV at room temperature. Similarly, eq 24 can be replaced by

$$\left(\frac{\epsilon_\nu}{\nu}\right)^{\mathrm{RBCT}} = \left(\frac{\epsilon_\nu}{\nu}\right)_{\max}^{\mathrm{RBCT}} \rho_{\mathrm{SC}} \int_{\epsilon_{\mathrm{bot}}^{\mathrm{CB}}}^{+\infty} \exp\left[-\frac{(\lambda - h\nu + \epsilon_i - e(E_{\mathrm{bot}}^{\mathrm{CB}} - E^0))^2}{4\lambda k_\mathrm{B}T}\right] \mathrm{d}\epsilon_i \tag{28a}$$

where

$$\int_{\epsilon_{\mathrm{bot}}^{\mathrm{CB}}}^{+\infty} \exp\left[-\frac{(\lambda - h\nu + \epsilon_i - e(E_{\mathrm{bot}}^{\mathrm{CB}} - E^0))^2}{4\lambda k_\mathrm{B}T}\right] \mathrm{d}\epsilon_i = \frac{\sqrt{\pi}}{2}(1 - \mathrm{erf}[h\nu - (\lambda - e(E_{\mathrm{bot}}^{\mathrm{CB}} - E^0))]) \tag{28b}$$

and

$$\left(\frac{\epsilon_\nu}{\nu}\right)^{\mathrm{BOCT}} = \left(\frac{\epsilon_\nu}{\nu}\right)_{\max}^{\mathrm{BOCT}} \rho_{\mathrm{SC}} \int_{-\infty}^{\epsilon_{\mathrm{top}}^{\mathrm{VB}}} \exp\left[-\frac{(\lambda - h\nu - \epsilon_i + e(E_{\mathrm{top}}^{\mathrm{VB}} - E^0))^2}{4\lambda k_\mathrm{B}T}\right] \mathrm{d}\epsilon_i \tag{29a}$$

where

$$\int_{-\infty}^{\epsilon_{\mathrm{top}}^{\mathrm{VB}}} \exp\left[-\frac{(\lambda - h\nu - \epsilon_i + e(E_{\mathrm{top}}^{\mathrm{VB}} - E^0))^2}{4\lambda k_\mathrm{B}T}\right] \mathrm{d}\epsilon_i = \frac{\sqrt{\pi}}{2}(1 + \mathrm{erf}\{h\nu - (\lambda + e(E_{\mathrm{top}}^{\mathrm{VB}} - E^0))\}) \tag{29b}$$

where erf is the error function[61] and the integral is carried out from e_{bot}, the bottom of the conduction band, to $+\infty$ for RBCT and from $-\infty$ to the top of the valence band for BOCT. Figure 10 contrasts the individual Gaussian component ϵ_i and the full absorption profile to be expected for a semiconductor.

Figure 7 and the dashed line in Figure 10 are essentially superposable, and either provides a useful prediction of the interfacial charge-transfer absorption profile.

It is worth noting that for the case of both metal and semiconductor bands an IFCTA profile such as Figure 7 or the dotted line in Figure 10 does not provide information about the electron-transfer reorganizational energy as directly as the spectra of binuclear, molecular, donor−acceptor pairs that exhibit absorption maxima rather than absorption plateaus. For this purpose, it is probably more useful to analyze the derivative of the profile with respect to energy because it is Gaussian with a maximum at $\lambda + \Delta G^\circ$ and $\Delta\nu_{1/2} = 2[4\ln(2)\lambda k_\mathrm{B}T]^{1/2}$.[54] Finally, we emphasize that we have *not* proposed a parallel between thermal and optical electron transfer for semiconductors, as was done for intramolecular electron transfer and electron transfer between a molecule and a metal. For a semiconductor electrode, thermal electron transfer is a carrier-dependent, complex phenomenon.[5,62,63] Moreover, it is questionable whether all

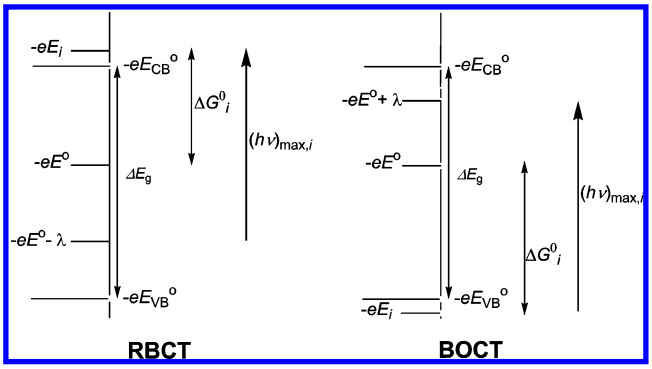

Figure 9. Energetics of RBCT and BOCT for a semiconductor with ΔE_g separating the top of the valence band and the bottom of the conduction band.

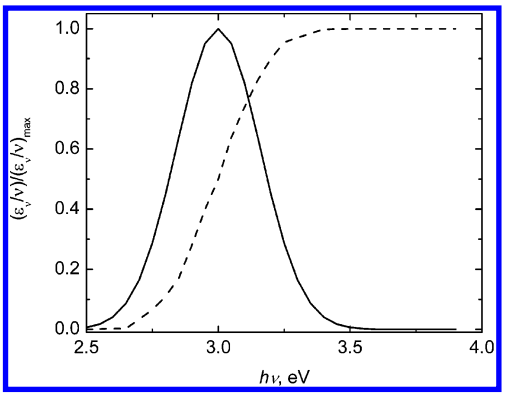

Figure 10. Relationship between the lowest-energy component in the molecule−semiconductor charge-transfer transition (Gaussian, solid line) and the overall absorption profile (eq 28). Parameters used: $\lambda = 0.5$ eV, $\Delta G^\circ = 2.5$ eV, $T = 298$ K.

charge-transfer processes between solutes and semiconductor electrodes should occur via the conduction band because the coupling to the conduction band should be weak. Rather it has been proposed that transfer via localized states may play an important role in many systems.[64]

D. Intensity Considerations. For optical interfacial charge transfer, the absorption intensity is determined by the product of the metal/semiconductor density of states and the square of the electronic coupling between the molecular species and the electronic levels of the band, the same parameters that (with the nuclear factor) determine the rate of thermal nonadiabatic electron transfer.

For each *i*th Gaussian component, the μ_{12} transition dipole moment $\langle\Psi_1|\mu|\Psi_2\rangle$ for the charge-transfer transition is[19,65]

$$\mu_{12} = \frac{H_{12}er}{\nu_{\max}} \tag{30}$$

where $\mu = -er$ is the electric dipole moment operator, H_{12} is the electronic coupling between states 1 and 2, and r is the distance over which electron transfer occurs. The maximum value of the ratio ϵ_ν/ν is given by[19,65]

$$\left(\frac{\epsilon_\nu}{\nu}\right)_{\max} = 2\pi^3 \frac{|\mu_{12}|^2}{[3 \times 10^3 \ln(10) c\sqrt{\pi\lambda k_\mathrm{B}T}]} \tag{31}$$

which can be combined with eq 30 to give the Mulliken−Hush expression[19] for $\epsilon_{\max}(M^{-1}\ \mathrm{cm}^{-1})$ at $(h\nu)_{\max}$,

$$\epsilon_{max} = \frac{4.9 \times 10^1 H_{12}{}^2 r^2}{\nu_{max} \lambda^{1/2}} \tag{32}$$

(energies in wavenumbers, r in Å, 298 K) provided that $(\epsilon_\nu/\nu)_{max} = \epsilon_{max}/\nu_{max}$, which is a good approximation when $\lambda \gg k_B T$.

Direct Coupling. It is normally assumed that the electronic coupling between a molecular reactant and an electrode is independent of the driving force for electron transfer—that is, independent of the metal/semiconductor level (also used by Hush in treating intensity as a function of overpotential[15]). It then follows from eq 32 that the intensities at the absorbance maxima for the transitions from (to) the ground-state minimum of Red (Ox) and energy levels ϵ_i and ϵ_j are related by

$$\frac{(\epsilon_{max})_j}{(\epsilon_{max})_i} = \frac{(rH_{12})_j^2 (\nu_{max} \lambda^{1/2})_i}{(rH_{12})_i^2 (\nu_{max} \lambda^{1/2})_j} \tag{33}$$

Thus, according to eq 35, for constant r, H_{12}, and λ the molar absorptivity must decrease to offset the increase in the energy of ν_{max}. As a consequence, the absorption profile for the direct coupling mechanism is expected to decrease gradually in intensity as $h\nu$ increases. Figure 11 illustrates this effect.

Thus, when the electronic coupling and transition moment are assumed to be independent of photon energy, a peaked, highly asymmetric absorption profile is predicted. The absorption peak is at ca. $\lambda + \Delta G^\theta + \sqrt{4\lambda k_B T}$

Superexchange Coupling. When the electron donor (reductant) or acceptor (oxidant) interacts with the metal/semiconductor through a bridging or tethering group (as in the case of ferrocene-terminated alkanethiols bonded to gold electrodes[2,3,66] or polypyridylruthenium(II) complexes attached via carboxylate substituents to titanium dioxide electrodes[67]), the presence of the bridge introduces an additional coupling mechanism. In the so-called superexchange mechanism,[68−70] the coupling of the initial and final states involves mixing with charge-transfer states deriving from electron transfer to or from bridging group B. Superexchange treatments have been applied to the problem of nonadiabatic thermal electron transfer to/from ferrocene thiols attached to Au[71,72] and Pt.[73]

Within a superexchange model H_{12}^{eff} is determined by the vertical energy separation between the initial and final states and the intermediate charge-transfer state at the equilibrium configuration of the initial state. (In contrast, for thermal electron transfer it is the vertical energy gaps at the reactant−product intersection configuration that determine the degree of mixing.)

$$H_{12}^{eff} = \frac{(H_{13})(H_{23})}{\Delta G_{eff}} \tag{34}$$

where

$$\frac{1}{\Delta G_{eff}} = \frac{1}{2}\left[\frac{1}{\Delta G_{13}} + \frac{1}{\Delta G_{23}}\right] \tag{35}$$

Contributions to ΔG_{eff} are obtained from the following relations and are shown in Figure 12.

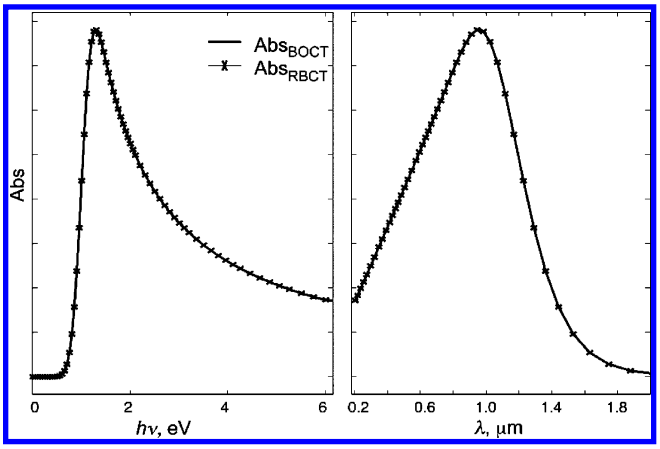

Figure 11. Intensity profile predicted by a Mulliken−Hush model. (Left) Absorbance vs energy; (right) absorbance vs wavelength. Parameters used: $\lambda = 0.5$ eV $= \Delta G^\theta$.

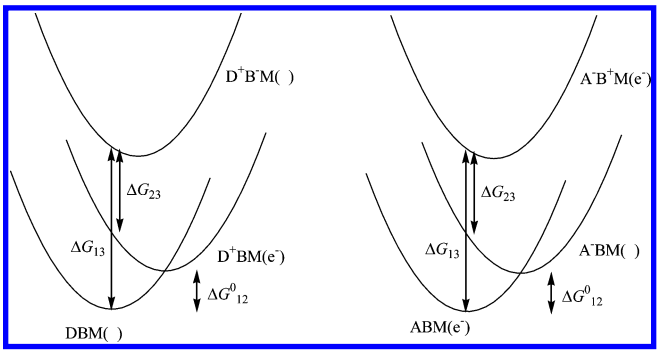

Figure 12. (Left) Energetics of superexchange coupling for RBCT, DBM( ) $\xrightarrow{h\nu}$ $D^+BM(e^-)$; mixing of initial and final states with the excited-state $D^+B^-M()$ is shown. (Right) Energetics of superexchange coupling for BOCT, ABM(e^-) $\xrightarrow{h\nu}$ A−BM( ); mixing of initial and final states with the excited-state $A^-B^+M(e^-)$

For RBCT,

$$\Delta G_{12}^0 = -e(E_i - E_D^0{}^{+/D})$$

$$\Delta G_{13} = -e(E_{B/B^-}^0 - E_D^0{}^{+/D}) + \lambda_B$$

$$\Delta G_{23} = e(E_i - E_{B/B^-}^0) - \lambda_D + \lambda_B$$

For BOCT,

$$\Delta G_{12}{}^0 = e(E_i - E_{A/A^-}^0)$$

$$\Delta G_{13} = e(E_B{}^{+}/B^0 - E_{A/A^-}^0) + \lambda_B$$

$$\Delta G_{23} = -e(E_i - E_B^0{}^{+/B}) - \lambda_A + \lambda_B$$

Because the superexchange contribution to the electronic coupling/absorption intensity increases as the energy gaps involving the bridge states diminish, there should be spectral regions in which the intensity of the absorption *increases* with $E(h\nu)$, in provocative contrast to the direct-coupling mechanism for which a falloff in intensity at high energy was predicted. For thermal electron transfer, it is recognized that when the bridge state is sufficiently low-lying it becomes necessary to employ a three-state model in which the electron (hole) is localized on the bridge.[19,70,74−76] The spectroscopic parallel of this phenomenon is that the bridge-based state is directly

accessed optically through

$$\mathrm{DBM}() \xrightarrow{h\nu} \mathrm{D^+B^-M}( )$$

charge-transfer absorption or

$$\mathrm{ABM}(e^-) \xrightarrow{h\nu} \mathrm{A^-B^+M}(e^-)$$

charge-transfer absorption. It may be anticipated that the interpretation of spectral intensity for RBCT/BOCT absorption enhanced by mixing with excited states of the bridge will be complicated by overlapping, intense excitations involving direct charge-transfer absorption of the bridge.

E. Conclusions. The parallel between the free-energy profiles of the rate constants for thermal intramolecular and interfacial charge transfer and the shapes of the corresponding charge-transfer absorption spectra has been explored within a classical, nonadiabatic framework. Although the nuclear factors (distribution functions) for thermal and optical charge transfers are identical, their electronic factors may differ. Provided that the electronic coupling elements are independent of the energy change, the electronic factors for the rate constants of a series of related electron-transfer reactions will be independent of the reaction driving force whereas the electronic factors for the associated optical electron-transfer processes (maxima of the individual charge-transfer absorption spectra) will decrease with increasing photon energy. This is most readily seen in the comparison of the free-energy profiles of charge-transfer rates at metal electrodes and the predicted interfacial spectra: Provided that H_{12} is constant, the rate constants will plateau, whereas the intensity of the corresponding interfacial charge-transfer absorption will decrease at high energy (short wavelength).

Acknowledgment. This research was carried out at Brookhaven National Laboratory under contract DE-AC02-98CH10886 with the U.S. Department of Energy, supported by its Division of Chemical Sciences, Office of Basic Energy Sciences, and at the California Institute of Technology by the Arnold and Mabel Beckman Foundation. We thank S. Feldberg for providing the program enabling the calculation of Figure 7 and S. Lymar, M. D. Newton, and M. Spitler for helpful discussions.

Note Added after ASAP Publication. This article was posted ASAP on the Web on 4/28/2005. A change was made in the paragraph preceding eq 33. The correct version was posted on 5/02/2005.

References and Notes

(1) Adams, D.; Brus, L.; Chidsey, C. E. D.; Creager, S.; Creutz, C.; Kagan, C. R.; Kamat, P. V.; Lieberman, M.; Lindsay, S.; Marcus, R. A.; Metzger, R. M.; Michel-Beyerle, M. E.; Miller, J. R.; Newton, M. D.; Rolison, D. R.; Sankey, O.; Schanze, K. S.; Yardley, J.; Zhu, X. *J. Phys. Chem. B* **2003**, *107*, 6668−6697.

(2) Smalley, J. F.; Finklea, H. O.; Chidsey, C. E. D.; Linford, M. R.; Creager, S. E.; Ferraris, J. P.; Chalfant, K.; Zawodzinsk, T.; Feldberg, S. W.; Newton, M. D. *J. Am. Chem. Soc.* **2003**, *125*, 2004−2013.

(3) Chidsey, C. E. D. *Science* **1991**, *251*, 919−922.

(4) Sikes, H. D.; Smalley, J. F.; Dudek, S. P.; Cook, A. R.; Newton, M. D.; Chidsey, C. E. D.; Feldberg, S. W. *Science* **2001**, *291*, 1519−1523.

(5) Lewis, N. S. *J. Phys. Chem. B* **1998**, *102*, 4843−4855.

(6) Vrachnou, E.; Vlachopoulos, N.; Grätzel, M. *J. Chem. Soc., Chem. Commun.* **1987**, 868.

(7) Lu, H.; Prieskorn, J. N.; Hupp, J. T. *J. Am. Chem. Soc.* **1993**, *115*, 4927−4928.

(8) Ghosh, H. N.; Asbury, J. B.; Weng, Y.; Lian, T. *J. Phys. Chem. B* **1998**, *102*, 10208−10215.

(9) Weng, Y.-X.; Wang, Y.-Q.; Asbury, J. B.; Ghosh, H. N.; Lian, T. *J. Phys. Chem. B* **2000**, *104*, 93−104.

(10) Huber, R.; Sporlein, S.; Moser, J. E.; Grätzel, M.; Wachtveitl, J. *J. Phys. Chem. B* **2000**, *104*, 8995−9003.

(11) Furube, A. K., R.; Yoshihara, T.; Hara, K.; Murata, S.; Arakawa, H.; Tachiya, M. *J. Phys. Chem. B* **2004**, *108*, 12583−12592.

(12) Robin, M. B.; Day, P. *Adv. Inorg. Chem. Radiochem.* **1967**, *10*, 247.

(13) Allen, G. C.; Hush, N. S. *Prog. Inorg. Chem.* **1967**, *8*, 391−444.

(14) Hush, N. S. *Prog. Inorg. Chem.* **1967**, *8*, 391−444.

(15) Hush, N. S. *Electrochim. Acta* **1968**, *13*, 1005−1023.

(16) Creutz, C. *Prog. Inorg. Chem.* **1983**, *30*, 1−73.

(17) Crutchley, R. J. *Adv. Inorg. Chem.* **1994**, *41*, 273−325.

(18) Demadis, K. D.; Hartshorn, C. M.; Meyer, T. J. *Chem. Rev.* **2001**, *101*, 2655−2686.

(19) Brunschwig, B. S.; Creutz, C.; Sutin, N. *Chem. Soc. Rev.* **2002**, *31*, 168−184.

(20) Curtis, J. C.; Meyer, T. J. *J. Am. Chem. Soc.* **1978**, *100*, 6284−6286.

(21) Billing, R. *Coord. Chem. Rev.* **1997**, *159*, 257−270.

(22) Kochi, J. K.; Sun, D.; Rosokha, S. V. *J. Am. Chem. Soc.* **2004**, *126*, 1388−1401.

(23) Nelsen, S. F. *Chem.−Eur. J.* **2000**, *6*, 581−588.

(24) Lambert, C.; Noll, G. *J. Am. Chem. Soc.* **1999**, *121*, 8434−8442.

(25) Coropceanu, V.; Gruhn, N. E.; Barlow, S.; Lambert, C.; Durivage, J. C.; Bill, T. G.; Nöll, G.; Marder, S. R.; Brédas, J.-L. *J. Am. Chem. Soc.* **2004**, *126*, 2727−2731.

(26) Nelsen, S. F.; Weaver, M. N.; Konradsson, A. E.; Telo, J. P.; Clark, T. *J. Am. Chem. Soc.* **2004**, *126*, 15431−15438.

(27) Endicott, J. F.; Uddin, M. J. *Coord. Chem. Rev.* **2001**, *219*, 687−712.

(28) Kolb, D. M.; Przasnyski, M.; Gerischer, H. *Z. Phys. Chem. Neue Folge* **1974**, *93*, 1−14.

(29) Khoudiakov, M.; Parise, A. R.; Brunschwig, B. S. *J. Am. Chem. Soc.* **2003**, *125*, 4637−4642.

(30) Yang, M.; Thompson, D. W.; Meyer, G. J. *Inorg. Chem.* **2002**, *41*, 1254−1262.

(31) Moser, J.; Punchihewa, S.; Infelta, P. P.; Grätzel, M. *Langmuir* **1991**, *7*, 3012−3018.

(32) Rajh, T.; Nedeljkovic, J. M.; Chen, L. X.; Poluektov, O.; Thurnauer, M. C. *J. Phys. Chem. B* **1999**, *103*, 3515−3519.

(33) Wang, Y.; Hang, K.; Anderson, N. A.; Lian, T. *J. Phys. Chem. B* **2003**, *107*, 9434−9440.

(34) Rodriguez, R.; Blesa, M. A.; Regazzoni, A. E. *J. Colloid Interface Sci.* **1996**, *177*, 122−131.

(35) Liu, Y. M.; Dadap, J. I.; Zimdars, D.; Eisenthal, K. B. *J. Phys. Chem B* **1999**, *103*, 2480−2486.

(36) Hush, N. S. *J. Electroanal. Chem.* **1999**, *460*, 5−29.

(37) Hush, N. S. *J. Electroanal. Chem.* **1999**, *470*, 170−195.

(38) Sutin, N. *Prog. Inorg. Chem.* **1983**, *30*, 441−498.

(39) Marcus, R. A.; Sutin, N. *Biochim. Biophys. Acta* **1985**, *811*, 265−322.

(40) Hush, N. S. *Prog. Inorg. Chem.* **1968**, *8*, 391−444.

(41) Bixon, M.; Jortner, J. In *Advances in Chemical Physics*; Prigogine, I., Rice, S. A., Eds.; Wiley-Interscience: New York, 2001; Vol. 106, pp 35−202.

(42) When ν changes little over the absorption band, a plot of absorbance or molar absorptivity versus ν can be approximated by a Gaussian. (See ref 19.)

(43) Gerischer, H. In *Electrochemistry*; Eyring, H., Ed.; Physical Chemistry, an Advanced Treatise; Academic Press: New York, 1970; Vol. 9A, pp 463−542.

(44) Gould, I. R.; Noukakis, D.; Gomezjahn, L.; Young, R. H.; Goodman, J. L.; Farid, S. *Chem. Phys.* **1993**, *176*, 439−456.

(45) Hopfield, J. J. *Proc. Natl. Acad. Sci. U.S.A.* **1974**, *71*, 3640−3644.

(46) Redi, M.; Hopfield, J. J. *J. Chem. Phys.* **1980**, *72*, 6651−6660.

(47) Devault, D. *Quantum-Mechanical Tunnelling in Biological Systems*; 2nd ed.; Cambridge University Press: Cambridge, U.K., 1984; p 73 ff.

(48) Bard, A. J.; Faulkner, L. R. *Electrochemical Methods*, 2nd ed.; Wiley: New York, 2001; pp 124−130.

(49) Matthews, D. *Aust. J. Chem.* **1994**, 2171−2186.

(50) Marcus, R. A. *J. Chem. Phys.* **1965**, *43*, 679−701.

(51) Gosavi, S.; Marcus, R. A. *J. Phys. Chem. B* **2000**, *104*, 2067−2072.

(52) Forster, R. J.; Faulkner, L. R. *J. Am. Chem. Soc.* **1994**, *116*, 5444−5452.

(53) Finklea, H. O.; Ravenscroft, M. S.; Snider, D. A. *Langmuir* **1993**, *9*, 223−227.

(54) Becka, A. M.; Miller, C. J. *J. Phys. Chem.* **1992**, *96*, 2657−2668.

(55) Xu, J.; Li, H.; Zhang, Y. *J. Phys. Chem.* **1993**, *97*, 11497−11500.

(56) Forster, R. J.; Loughman, P.; Keyes, T. E. *J. Am. Chem. Soc.* **2000**, *122*, 11948−11955.

(57) Nozik, A. J.; Memming, R. *J. Phys. Chem.* **1996**, *100*, 13061−13078.

(58) Bard, A. J.; Faulkner, L. R. *Electrochemical Methods*, 2nd ed.; Wiley: New York, 2001.
(59) Robinson, D. B.; Chidsey, C. E. D. *J. Phys. Chem. B* **2002**, *106*, 10706−10713.
(60) Nahir, T. M. *J. Electroanal. Chem.* **2002**, *518*, 47−50.
(61) Bard, A. J.; Faulkner, L. R. *Electrochemical Methods*, 2nd ed.; Wiley: New York, 2001; pp 778−780.
(62) Bard, A. J.; Faulkner, L. R. *Electrochemical Methods*, 2nd ed.; Wiley: New York, 2001; p 752.
(63) Royea, W. J.; Fajardo, A. M.; Lewis, N. S. *J. Phys. Chem. B* **1997**, *105*, 11152−11159.
(64) Memming, R. In *Electroanalytical Chemistry; A Series of Advances*; Bard, A. J., Ed.; Marcel Dekker: New York, 1979; Vol. 11, pp 1−84.
(65) Atkins, P. W.; Friedman, R. S. *Molecular Quantum Mechanics*, 3rd ed.; Oxford University Press: Oxford, U.K., 1997; p 509.
(66) Smalley, J. F.; Feldberg, S. W.; Chidsey, C. E. D.; Linford, M. R.; Newton, M. D.; Liu, Y.-P. *J. Phys. Chem.* **1995**, *99*, 13141.
(67) O'Regan, B.; Grätzel, M. *Nature* **1991**, *353*, 737−740.
(68) McConnell, H. M. *J. Chem. Phys.* **1961**, *35*, 508.
(69) Cave, R. J.; Newton, M. D. *J. Chem. Phys.* **1997**, *106*, 9213−9213.
(70) Creutz, C.; Newton, M. D.; Sutin, N. *J. Photochem. Photobiol., A* **1994**, *82*, 47−59.
(71) Hsu, C.-P.; Marcus, R. A. *J. Chem. Phys.* **1997**, *106*, 584−598.
(72) Hsu, C.-P. *J. Electroanal. Chem.* **1997**, *438*, 27−35.
(73) Gosavi, S.; Qin Gao, Y.; Marcus, R. A. *J. Electroanal. Chem.* **2001**, *500*, 71−77.
(74) Cave, R. J.; Newton, M. D. *Chem. Phys. Lett.* **1996**, *249*, 15.
(75) Newton, M. D. *Adv. Chem. Phys.* **1999**, *106*, 303−375.
(76) Lambert, C.; Amthor, S.; Schelter, J. *J. Phys. Chem. A* **2004**, *108*, 6474−6486.